Ab initio investigation of molecular hydrogen physisorption on graphene and carbon nanotubes

D. Henwood* and J. David Carey†

Advanced Technology Institute, School of Electronics and Physical Sciences, University of Surrey, Guildford GU2 7XH, United Kingdom

(Received 3 October 2006; revised manuscript received 4 April 2007; published 13 June 2007)

Density-functional theory is used to investigate hydrogen physisorption on a graphene layer and on single wall carbon nanotubes. Both external and internal adsorption sites of (9, 0) and (10, 0) carbon nanotubes have been studied with the hydrogen molecular axis oriented parallel or perpendicular to the nanotube wall. A range of hydrogen molecule binding sites has been examined and it is found that hydrogen binds weakly to each of the graphitic structures and at all adsorption sites examined. Calculations using different functionals reveal that the binding energies are a factor of 2 larger for hydrogen bound inside the nanotubes than for adsorption outside the nanotubes or on the graphene layer. Furthermore, configurations of the hydrogen molecular axis parallel to the nanotube wall or graphene layer bind more effectively than configurations where the axis is normal to the carbon nanostructures. The differing behavior between the carbon nanostructures is attributed to the curvature of the structure and the hydrogen-carbon electron interactions, where analysis of the electron density reveals evidence of charge redistribution with little charge transfer. The potential of hydrogen physisorption to carbon nanostructures for hydrogen storage and delivery is also discussed.

DOI: 10.1103/PhysRevB.75.245413 PACS number(s): 73.22.−f, 71.15.Mb

I. INTRODUCTION

Hydrogen has significant potential as a source of energy for the future, where it can be used in efficient fuel cell technology to produce electricity particularly for mobile applications. It has been proposed that a stored mass of 5–10 kg of hydrogen can be used to power road vehicles over a distance of approximately 500 km.[1] Molecular hydrogen may also be used as a fuel in modified internal combustion engines. The difficulties associated with hydrogen use stem from limited storage capabilities and delivery. Liquefaction of hydrogen at cryogenic temperatures is a technique that exists in a mature form. However, the cryogenic vessels that are currently available are considered too bulky to be utilized in vehicles. Furthermore, a large amount of energy is needed to liquify hydrogen, potentially rendering the system inefficient. Gas compression, another established technology, is also judged to be unsuitable as only small amounts of hydrogen can be stored in bulky containers. Further complications arise as the storage vessels, in both systems, are prone to failure due to hydrogen attack, usually after long exposure inherent in vehicular storage. The U.S. Department of Energy (DOE) has specified targets for hydrogen storage research.[1] These include high storage as a percentage of the system weight, a high density of hydrogen, and a refueling rate of 1.5 kg/min by 2010.[1] Both gas compression and liquefaction are considered to be the current state-of-the-art storage systems for hydrogen[2] though neither has met the capacity target of 4.5 wt % by 2005 set by the DOE. Solid-state storage, in which the hydrogen is stored in lattice interstitial sites, is a solution that may provide high storage densities at these conditions.[1] Metals and metal alloys have been tested as storage materials but none of over 2000 known materials, which can form metal hydrides, have been able to meet all of the DOE targets although $NaBH_4$ meets many of the requirements by hydrolysis of the hydride.[3] Some metal hydrides have a high hydrogen wt % capacity, such as MgH_2 and LiH_2 (7–13 wt %) (Ref. 4) and $NaAlH_4$ (5.6 wt %).[4] However, these hydrides have high desorption temperatures, for example, MgH_2 desorbs hydrogen at 573 K.[5] Ideally, a hydride decomposition temperature comparable to the waste heat of the fuel cell [typically 60 to 120 °C (Ref. 6)] is desired. Hydrides that desorb easily at this temperature adsorb between 1 and 3 wt %.[4] Some hydrides also exhibit adsorption and/or desorption kinetics,[4] which would necessitate the use of detachable canisters that can be refilled at factories rather than at the roadside.

Gas-on-solid adsorption, particularly using nanostructured materials, has earned considerable attention for its safe nature and the potential for a high storage density of hydrogen. In addition to the DOE requirements for storage, the interaction, or binding, energy between hydrogen and the storage material must be small compared with covalent bond strengths as hydrogen must be easily accessible for delivery. It has been shown that the quantity of delivered hydrogen is less than the total storage capacity.[1,7] If the interaction between the adsorbate and the adsorbing material is large, a quantity of the adsorbate can be left behind in the storage vessel after exhaustion. Physisorption, mainly dependent on electrostatic and weak van der Waals interactions, would be preferable to chemisorption as the latter requires a large input of energy to overcome the chemical bonds between the adsorber and the hydrogen. Desorption of hydrogen chemically bonded to single-walled carbon nanotubes (SWNTs) requires a temperature greater than 600 K, rendering chemisorption impractical for mobile hydrogen storage.[7] In spite of this, carbon nanostructures, such as graphite, individual graphene layers, and carbon nanotubes, appear to be ideal storage materials as they possess considerable surface area. The transport of hydrogen through these nanostructures is also of importance to potential storage systems. However, transport is out of the scope of this study which focuses on the conditions for adsorption to take place.

A graphene sheet may store hydrogen on both sides of its structure. Likewise, hydrogen may be stored both outside and inside carbon nanotubes. There is considerable debate within the literature as to whether these structures are physi-

cally capable of storing a practically viable amount of hydrogen within the confines of the accepted operating conditions. One previous experimental study has shown that hydrogen can be stored at room temperature and pressure.[8] By contrast, other experimental studies have concluded that storage can only occur at cryogenic temperatures[9,10] and/or high pressures.[9–11] Theoretical studies have been carried out, using several different modeling techniques on a wide range of carbon nanostructures, and the results have varied significantly. By means of molecular dynamics and density-functional theory (DFT) simulations, it has been calculated that atomic hydrogen chemically binds to carbon atoms in nanostructures with binding energies of the order of 1 eV.[12] Molecular hydrogen physisorption onto graphene has been examined using DFT (Refs. 13 and 14) with binding energies of the order of 80–90 meV: an order of magnitude less than that of atomic hydrogen binding energies. Okamoto and Miyamoto found that H_2 oriented parallel to the graphene is more stable than normally oriented H_2.[13] Calculations using modified Lennard-Jones potentials have shown binding energies of 200 meV for molecular hydrogen adsorbed externally on a (9, 9) nanotube and 40 meV for internally adsorbed molecular hydrogen.[15] Molecular dynamics has been used to demonstrate that molecular hydrogen adsorption on SWNTs can occur up to temperatures of 600 K with binding energies of 300 meV.[16] Arellano *et al.* used molecular dynamics to investigate hydrogen physisorption onto armchair nanotubes.[12] Physisorption was found to be weak with internal binding energies larger than external energies. Larger internal hydrogen binding energies were also demonstrated by Han and Lee,[17] for (10, 0) zigzag nanotubes, in contrast to Kostov *et al.*[15] However, Han contradicts Okamoto by calculating that hydrogen oriented with its axis perpendicular to the nanotube surface is weaker than parallel orientations. The heat of adsorption of hydrogen on carbon nanostructures ranges from 40 to 80 meV per hydrogen molecule,[7] which shows a weak interaction between molecular hydrogen and carbon nanostructures compared with covalent bond strengths of 3.5 eV per C–H bond. Optimum delivery of an adsorption-based system functioning at near sea-level pressures (storage pressure of 30 bar and exhaustion pressure of 1.5 bar) is calculated, from the Langmuir isotherm, at 63.5% of stored hydrogen. To obtain this delivery from a carbon nanostructure, the temperature must be as low as 115 K (Ref. 7), reiterating the need for weak interaction, i.e., physisorption, between these forms of hydrogen and carbon.

This paper reports a comprehensive study, using DFT calculations to investigate the physisorption of molecular hydrogen onto various adsorption sites and orientations on carbon nanostructures. The ability of a graphene sheet to store hydrogen will be compared with that of SWNTs. Segments of a (10, 0) and a (9, 0) carbon nanotube were used to simulate hydrogen physisorption on SWNTs. Both have a zigzag geometrical structure with similar diameters: 7.9 and 7.1 Å for the semiconducting (10, 0) and metallic (9, 0) nanotubes, respectively. This affords a comparison of hydrogen adsorption onto tubes with differing electronic structures but near identical diameters.

II. SIMULATION DETAILS AND LATTICE COORDINATION

A. Simulation details

Density-functional theory has a relatively low computational cost, compared with other quantum mechanical approaches, which makes it an ideal method for calculating the electronic structure of many-atom systems. However, while the electronic structure, due to the kinetic and potential energies, can be trivially calculated using a free-electron gas model, the exchange and correlation energy functions are not known explicitly.[18] Many approximations have been put forward to calculate the exchange and correlation energies which have been broadly divided into two main categories. The local density approximation (LDA) assumes that the exchange and correlation energies are a function of the electron density at the point of evaluation only. The generalized gradient approximation (GGA), however, takes into account the gradient of the electron density at the point of evaluation. LDA has a tendency to overestimate the binding energies between two molecules, compared with experimental results.[17,19] Conversely, GGA tends to underestimate binding energies predicting a shallow or flat adsorption well.[19,20] It is known that no DFT functional accurately describes all the characteristics of molecular interactions,[21] especially van der Waals (vdW) interactions.[12,20,22,23] However, in some cases, the LDA has given good agreement with experimental results through fortuitous error cancellations between exchange and correlation energy approximations.[20,23,24] A van der Waals corrected DFT functional gives the binding energy of H_2 to a graphene layer, as 60 meV falling between the uncorrected LDA (86–92 meV) and GGA (4 meV) functionals.[23] In light of this, DFT is able to predict the chemical and physical properties of many-atom systems to a reasonable accuracy. Therefore, since the vdW corrected result is comparable to the LDA and GGA results in the case of hydrogen physisorption on graphene, the uncorrected functionals will be utilized within this study. The discussion of the results will emphasize the trends in the binding energies as much as the actual values themselves.

The DFT package utilized for this study was Dmol^3 used through the MS MODELING SUITE.[25] Initially, a comparison is made between the LDA Vosko-Wilk-Nusair (VWN),[26] and the GGA Perdew-Wang[27] (PW91) and Perdew-Burke-Ernzerhof[28] (PBE) functionals using a double numerical plus polarization basis set. All electrons were included in the calculations with a basis set cutoff of 4.0 Å. The binding energy (E_{bind}) of H_2 to the nanotube or graphene can be calculated from the molecular energies:

$$E_{bind} = E_{\text{C–H}_2} - E_{\text{C}} - E_{\text{H}_2}, \tag{1}$$

where E_{C} represents the total energy of the carbon structure (graphene layer or nanotube), E_{H_2} is the energy of the isolated hydrogen molecule, and $E_{\text{C–H}_2}$ is the total energy of the hydrogen-carbon system. The electron density surrounding the molecules is also obtained with all of the carbon-carbon bonds entirely sp^2 hybridized. In addition, all dangling bonds, in both the graphene plate and the two nanotube segments, were hydrogen terminated to minimize the system

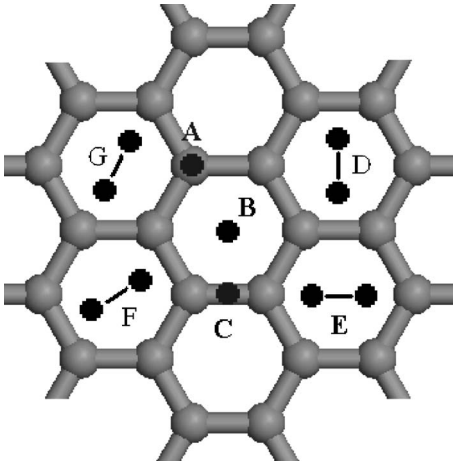

FIG. 1. Physisorption sites for a hydrogen molecule on a graphene layer. All C–C bonds are sp^2 hybridized.

energy and ensure swift self-consistent field convergence. The nanotubes were fixed at lengths of approximately 11 Å consisting of 120 and 108 carbon atoms for the (10, 0) and (9, 0), respectively. This length was chosen as it was found that hydrogen adsorption was affected by the terminating hydrogen atoms for shorter segments of nanotube. Electron-density data are arranged in three-dimensional arrays with 0.1 Å spacing between data points.

B. Hydrogen physisorption on graphene

A hexagonal plate consisting of 96 carbon atoms was chosen to represent a graphene sheet. Binding energies were evaluated by single point energy calculations on static configurations of the graphene-hydrogen system. Bond lengths are measured as 0.74 and 1.42 Å for H–H and sp^2 carbon bonds, respectively, which compare well with the experimental values of 0.74 Å for H–H (Ref. 29) and 1.415 (Ref. 30) or 1.41 Å (Ref. 31) for C–C bonds. For comparison, the atomic positions of all atoms were relaxed before and after the introduction of the hydrogen molecule. Calculated C–C bond lengths were only altered by a maximum of 0.03 Å when optimized by the LDA VWN functional and 0.003 Å by the GGA PW91 functional. The H–H bond lengths were altered by approximately the same amount to 0.77 and 0.75 Å for LDA VWN and GGA PW91, respectively. The energetics of the relaxed structures was then compared with their unoptimized counterparts. The separation between the graphene sheet and the hydrogen molecule's center of mass was varied between 2 and 7 Å. Several adsorption sites were studied with the axis of the hydrogen molecule aligned parallel, or perpendicular, to the graphene surface (Fig. 1). H_2 is placed above, or as close to, the center of the graphene plate to avoid edge effects on the hydrogen-graphene binding energies. Sites A–C are aligned with the hydrogen molecular axis normal to the graphene surface, while sites D–G are aligned with the hydrogen axis parallel to the graphene surface. Hydrogen is placed above a carbon atom (site A), above the center of a hexagon of carbon atoms (site B), and above the midpoint of a C–C bond (site C). For site D, the hydrogen lies across the midpoints of the C–C bonds and for site E, the hydrogen lies across two opposing carbon atoms. Site F represents a hydrogen molecule, parallel to the graphene layer, which is rotated through 60°, about the hydrogen center of mass, from site D. Site G is related to site E by the same 60° rotation. Thus, as the graphene plate has sixfold rotational symmetry, adsorption sites D and F should have identical binding energies, as should sites E and G. Calculations for these pairs of adsorption sites act as an internal check of variations in results from the DFT code.

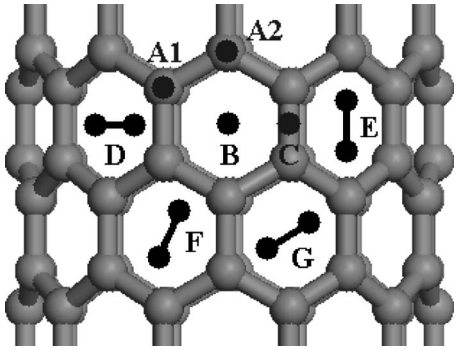

FIG. 2. Physisorption sites for a hydrogen molecule on a segment of a (10, 0) carbon nanotube. All C–C bonds are sp^2 hybridized.

C. Hydrogen physisorption on single wall carbon nanotubes

Adsorption sites on the nanotubes are comparable to the sites for the graphene plate (Fig. 2). In this case, the separation is now measured between the center of mass of the hydrogen molecule and the nanotube wall. All of the adsorption site designations are identical to that of their graphene counterparts. These adsorption site locations are also used to position the H_2 on the inside of the nanotube in order to include internally adsorbed H_2. As previously stated, for graphene adsorption, sites D and F should give identical binding energies, as should sites E and G. However, the curvature of the nanotube induces some sp^3 rehybridization effects that are absent in graphene. Bond angles between carbon atoms decrease with increasing curvature. This causes the delocalized ring of electrons in the π orbitals to become less delocalized above carbon atoms altering the electron density of the carbon nanotube. Consequently, the binding properties of the H_2 will change with the electron density as physisorption is governed by electrostatic forces and van der Waals (e.g., induced dipole-induced dipole). The underlying carbon structure for sites D–G, although identical for graphene, now has differing curvatures on the nanotube. However, as bond angles between carbon atoms change by 2° from graphene to nanotube compared with 11° for graphene to fully sp^3 hybridized diamond, the hydrogen binding energies are not expected to vary significantly. For unoptimized nanotubes, the C–C bonds were measured at 1.41 Å and the H–H bonds remain fixed at 0.74 Å. When relaxed, the nanotube's atomic positions were found to change negligibly with respect to a reference carbon atom. For the case of sites B–G, the hydrogen can be placed di-

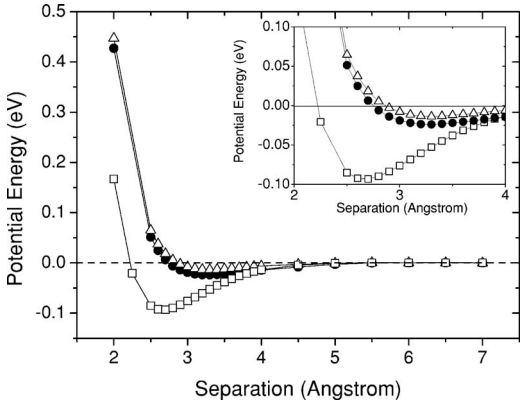

FIG. 3. Variation of potential energy with the separation between the graphene sheet and the center of mass of the hydrogen molecule in site D using the LDA VWN functional (□), the GGA PW91 functional (●), and the GGA PBE functional (△). Inset: close up of the potential-energy minima.

rectly at the midpoint of the nanotube axis eliminating effects of antisymmetry caused by the terminating hydrogen. The individual sites of A1 and A2 are included to observe any change in the hydrogen binding energies due to the nanotube termination effects.

III. RESULTS AND DISCUSSION

A. Adsorption on graphene

Figure 3 shows the potential energy plotted as a function of the graphene-hydrogen separation, for adsorption site D: the hydrogen molecule parallel to the unoptimized graphene layer, lying across two opposing C–C bond midpoints. All three DFT functionals show binding between H_2 and the graphene layer. Calculations with the LDA VWN functional give a binding energy of 93 meV at a separation of 2.7 Å. Both GGA functionals, PW91 and PBE, show lower binding energies of 23 and 13 meV, respectively. The binding energy calculated by LDA, 93 meV, is similar to that found by Arellano *et al.*, 86 meV, for H_2 adsorbed onto graphene, parallel to the surface.[14] The calculations using GGA functionals give similar binding energies to those of Han *et al.*, but are smaller than the 34 meV binding energy of hydrogen oriented normal to the (10, 0) nanotube, using the PW91 functional. Both GGA functionals show the hydrogen binding at a distance of 3.3 Å: this is farther from the wall than for LDA.

The curves in Fig. 3 show the typical form of a Lennard-Jones potential: an attractive region at long range that turns and becomes repulsive at short separations. At large separations, the interaction energy is small and grows steadily negative (attractive) as the hydrogen molecule is moved closer to the graphene layer. As the hydrogen passes the binding-energy minima, the Pauli repulsion interactions start to dominate. The attraction between H_2 and the graphene layer is due to interaction between the wave functions of the

TABLE I. Separations and binding energies of molecular hydrogen to the 96-atom graphene layer. The separation distances are measured from the graphene surface to the center of mass of the H_2 molecule.

Adsorption site	LDA functional		GGA functional	
	Sep (Å)	E_{bind} (meV)	Sep (Å)	E_{bind} (meV)
A	2.9	75.50	3.5	22.43
B	2.8	86.83	3.4	22.17
C	2.9	76.41	3.5	22.38
D	2.7	93.13	3.3	23.82
E	2.7	93.10	3.3	23.72
F	2.7	93.13	3.3	23.80

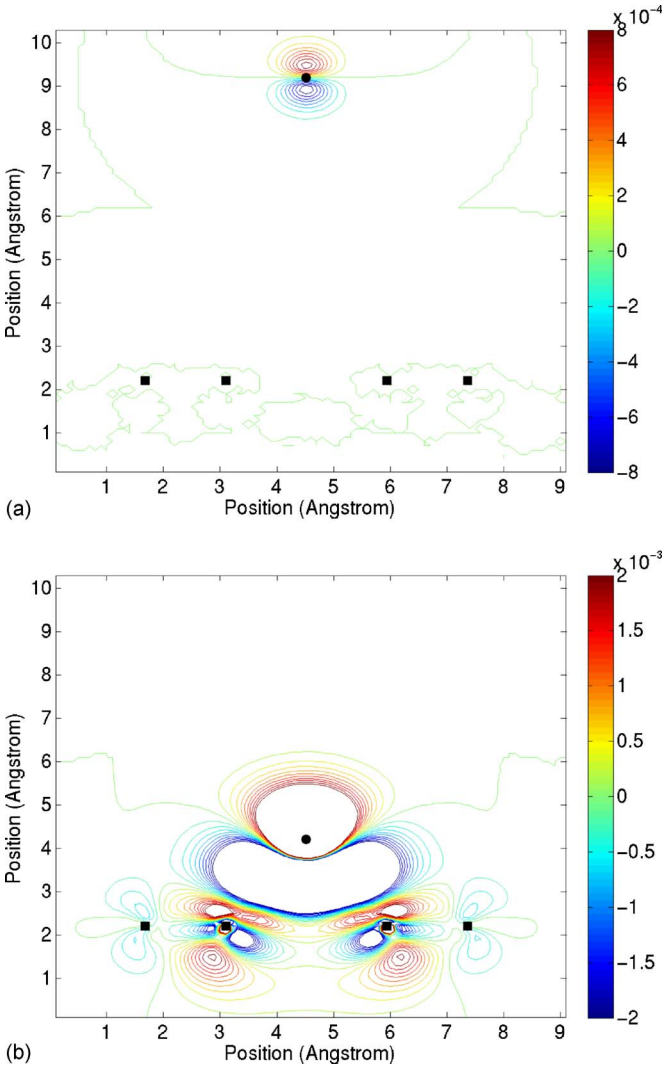

FIG. 4. (Color online) Contour map of the change in electron density for a hydrogen molecule placed (a) 7 Å and (b) 2 Å from, and parallel to, the graphene sheet surface across the C–C bond midpoints (adsorption site D). The view is in the plane of the graphene layer, looking end on to the hydrogen molecule (black circle located at the top of the figure). Four carbon atoms in the graphene matrix are labeled by black squares at the bottom of the figure. Scale bar is in units $e/Å^3$.

two molecules, with electrons in the σ molecular orbital of the H_2 overlapping with the electrons in the π state of the graphene to form bonding and antibonding states. As the hydrogen approaches the graphene surface, this interaction is initially attractive as the electron probability between the two molecules is enhanced. However, this interaction leads to the simultaneous decrease in the energy of the bonding level and rapid increase in the energy of the antibonding state. The repulsive force due to the filled antibonding state pushes the molecules apart forming an energy barrier which, if overcome, would dissociate the hydrogen allowing chemisorption to the graphene.

Optimization of the graphene structure with adsorbed hydrogen shows that when the hydrogen molecule is at large separation, the position of the hydrogen molecule changes negligibly with respect to the unoptimized position. At separations less than the stable binding distance, taken from the static calculations, the hydrogen molecule is pushed away from the graphene surface toward the stable binding separation. When the hydrogen molecule is at separations slightly greater than the stable binding separation, H_2 is pulled toward the graphene surface. The magnitude of the H_2 position change, upon optimization, is found to be dependent on the original separation, decreasing as the original position of the hydrogen molecule approaches the stable binding separation. These findings correlate with the predicted behavior of a hydrogen molecule placed on the interaction potentials of Fig. 3. Hydrogen molecule orientation does not change on optimization which signifies that moving between orientations requires energy to overcome local energy barriers.

The binding energies, and H_2-graphene separation, for adsorption sites A–F, are shown in Table I. It is known that the GGA PBE functional gives a higher mean absolute deviation from experimental values than the PW91 functional.[18] Since the PW91 functional calculates the binding energies to be more stable than those calculated using PBE, and that they are closer to the vdW corrected calculations, the results of hydrogen adsorption on graphene and nanotubes have been generated using only the LDA VWN and GGA PW91 functionals. In addition, although the binding energies calculated from the VWN and PW91 functionals differ by ~80 meV, the vdW corrected DFT binding energy of 60 meV falls between the binding energies found here. Given this fact and the small differences compared to covalent bond strengths, the uncorrected functionals are considered acceptable to investigate the trends in binding energy of vdW interactions between graphitic substances and hydrogen molecules. We have found that geometry optimizations act only to give a small correction of the hydrogen physisorption energies. Binding-energy minima calculated from optimized structures were found to be lowered by 13 and 2 meV for the LDA and GGA functionals and all graphene adsorption sites. It is, therefore, noted that the trend in binding energies for the different sites is the same between optimized and unoptimized structures. These corrections are within the errors of DFT when compared with the vdW corrected values and thus unoptimized structures can be used to study the trends in hydrogen physisorption. Sites D and F differ by 0.02 meV showing that the graphene plate is indeed symmetrical under DFT conditions.

Configurations where the axis of the hydrogen molecule is parallel to the surface (adsorption sites D–G) bind more strongly than axis perpendicular configurations. On average, the binding energies are 13.5 and 1.5 meV larger for the LDA and GGA functionals, respectively. The larger binding energies of the parallel configurations can be explained by the nature of the hydrogen molecule's electronic structure. As the electron cloud of H_2 is ellipsoidal, the center of mass of a hydrogen molecule, aligned parallel to the graphene, can approach closer to the surface before it experiences the same interaction as a perpendicularly oriented molecule. The two hydrogen atoms are now at the same distance from the surface and, therefore, both contribute the same interaction effectively doubling the graphene-hydrogen interaction strength. Thus, the potential well for hydrogen interaction becomes deeper for hydrogen molecules oriented parallel to the graphene-layer. Average graphene-hydrogen separations are slightly smaller for parallel configurations of the hydrogen when either functional is used to calculate the binding energies. Changes in the electron density illustrate the inter-

TABLE II. Separations and binding energies of molecular hydrogen outside the (10, 0) and (9, 0) SWNTs. The separation distances are measured from the nanotube wall to the center of mass of the H_2.

	(10, 0)				(9, 0)			
	LDA functional		GGA functional		LDA functional		GGA functional	
Adsorption site	Sep (Å)	E_{bind} (meV)	Sep (Å)	E_{bind} (meV)	Sep (Å)	E_{bind} (meV)	Sep (Å)	E_{bind} (meV)
A1	2.9	62.87	3.4	20.74	2.9	62.65	3.4	20.63
A2	2.9	63.13	3.5	20.77	2.9	62.80	3.5	20.74
B	2.7	79.20	3.4	20.70	2.7	79.75	3.4	20.78
C	3.0	60.34	3.5	20.15	3.0	59.94	3.4	19.98
D	2.6	82.59	3.3	21.36	2.6	82.48	3.3	21.37
E	2.5	89.98	3.2	22.28	2.5	91.99	3.2	22.56
F	2.6	88.03	3.2	22.05	2.5	89.24	3.2	22.26
G	2.6	84.45	3.2	21.59	2.6	84.83	3.3	21.61

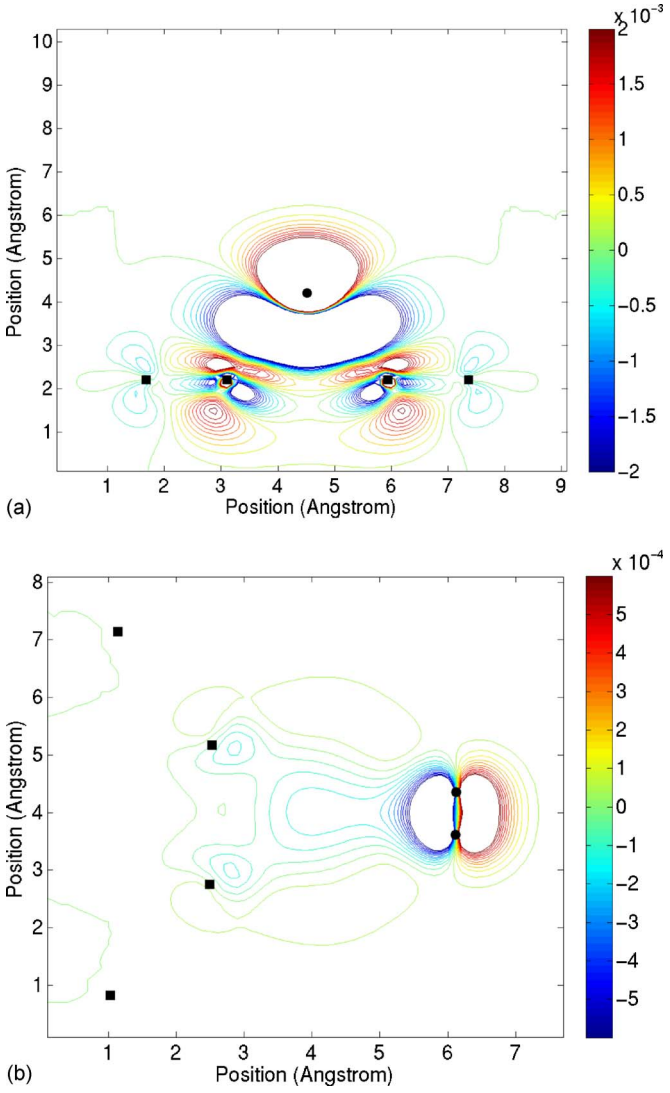

FIG. 5. (Color online) Contour map of the change in electron density for a hydrogen molecule placed (a) adjacent to a graphene layer at adsorption site D and (b) adjacent to a (10, 0) carbon nanotube at adsorption D. In (a), the H_2 is positioned 3.3 Å from the graphene layer. In (b), the H_2 is positioned 3.5 Å from the nanotube surface. The H_2 is parallel to the surface of both carbon nanostructures. The view of (a) is in the plane of the graphene layer, while the view of (b) is looking down the nanotube axis. Hydrogen atoms are denoted by black circles. Black squares denote carbon atoms. Scale bar is in units $e/Å^3$.

actions between the graphene and hydrogen molecules. Specifically, they illustrate how the electronic structure is distorted by the two molecule's proximity to one another. Figures 4(a) and 4(b) show contour maps of the change in electron density of the graphene-hydrogen system at separations of 7 and 2 Å for adsorption site D. These represent the electron density of the system, calculated using the GGA PW91 functional at a large separation [Fig. 4(a)] and at small separation, respectively [Fig. 4(b)]. LDA VWN electron-density plots are not shown as they were found to be very similar to the GGA PW91 plots. Figure 4(a) shows that an induced dipole is established on the hydrogen molecule at large separation. Note that the changes in electron density at this distance are of the order of 10^{-4} $e/Å^3$ indicating a weak dipole. This does, however, confirm the existence of a small but finite attractive force even at large separation. Figure 4(b) shows that at small separations, the electron density becomes highly distorted compared with the molecule's separation. While the range in electron density change of Fig. 4(b) is kept at 10^{-3} $e/Å^3$ to show the detail in the electronic structure, the electron-density change actually raises to ± 0.02 $e/Å^3$. These plots of the change in electron density have shown evidence of significant charge redistribution, particularly as the hydrogen molecule is brought close to the surface of the graphitic nanostructure. However, there is no evidence of charge transfer between the graphitic and hydrogen molecules. The proximity of contour lines between the hydrogen and graphene molecules indicates a large gradient in the electron density, which will result in a large electric field at that point. This signifies an unstable arrangement as the molecules will move to reduce these large intermolecular fields.

Turning to the specific nature of the van der Waals interactions, it is evident from Fig. 4(a) that the presence of the graphene layer alters the electron density surrounding the H_2 molecule, even to a distance of 7 Å. For example, at this distance, the potential energy is calculated to be about −0.16 meV. We can exclude both dipole-dipole and dipole-induced multipole interactions due to the absence of a permanent dipole in either H_2 or graphene. In terms of induced dipole-induced dipole interactions, we calculate a potential energy of −0.25 meV, for H_2 adsorbed at site D, at a separation of 7 Å, assuming polarizabilities of 1.7×10^{-41} and 3.4×10^{-39} J^{-1} C^2 m^2 for the hydrogen molecule and the 96-atom graphene layer, respectively.[32] For the quadrupole-quadrupole interactions, the potential energy is −0.74 meV, assuming quadrupole moments of 1.65×10^{-40} and 1.89×10^{-37} C m^2 for the H_2 and graphene, respectively. Both of these potential energies are comparable to the value calculated above. We can exclude quadrupole-induced quadrupole interactions, since this produces a potential energy of −36.6 meV, significantly greater than the calculated value at a separation of 7 Å.

These results show that hydrogen can physisorb to a single graphene layer with weak binding energies. Configurations where the axis of the hydrogen molecule is parallel to the graphene are favored. Relaxation of the atomic positions in the graphene-H_2 system serves to increase the hydrogen binding energies by a small correction factor across all the adsorption sites studied.

B. Adsorption on single wall carbon nanotubes

Binding energies, for hydrogen adsorbed externally on the (10, 0) and (9, 0) nanotubes using the LDA VWN and the GGA PW91 functionals, are displayed in Table II along with the separation between the hydrogen molecule's center of mass and the nanotube wall. The general trend observed for the graphene plate is recreated here: parallel configurations are more stable than normal orientations by averages of 20.4 and 1.3 meV for LDA and GGA functionals, respectively. This result directly contradicts the result of Han *et al.* found

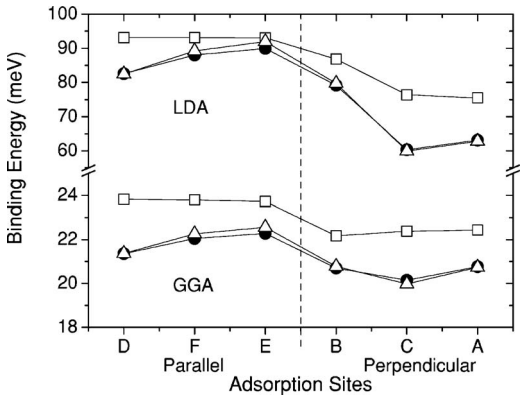

FIG. 6. Variation of binding energies for all carbon nanostructures calculated using the LDA VWN and GGA PW91 functionals. The adsorption sites are listed for binding energies of hydrogen to graphene (□), (10, 0) carbon nanotube (●), and (9, 0) carbon nanotube (△).

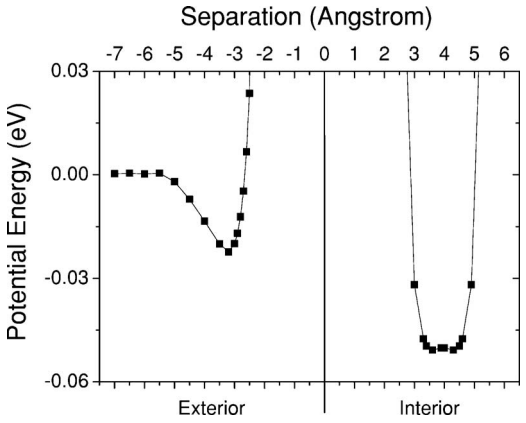

FIG. 7. Potential energy as a function of distance from the (10, 0) nanotube wall. A hydrogen molecule is placed in adsorption site E: parallel to the nanotube surface and the axis of the nanotube.

using the GGA PW91 functional on a (10, 0) nanotube. There is no significant difference in terms of binding energies or hydrogen-nanotube separation distances between the (10, 0) and (9, 0) nanotubes, indicating that the change in curvature between these two nanotubes has little effect on the binding energies of *externally* physisorbed hydrogen. With a difference in diameter of 0.8 Å, the change in curvature between the (10, 0) and (9, 0) nanotubes is small compared with the curvature difference between graphene and the nanotubes. However, the physisorption of hydrogen is affected by the curvature of nanotubes when evaluated against graphene. Average binding energies are approximately 10 and 2 meV lower than graphene binding energies for the LDA and GGA functionals, respectively. This is due to reduced interaction between the hydrogen molecule and the nanotube. Electronic wave functions spread out from graphene with a uniform distribution that minimizes the graphene's system energy. For the nanotubes, the electron wave functions can spread out radially, further reducing the system energy. Consequently, the electron wave functions external to the nanotube, occupy a greater volume of space thereby weakening the interaction with the unchanged electronic structure of the H_2. The weakened interaction reduces the binding energy of hydrogen to nanotubes compared with the hydrogen-graphene binding. In Fig. 5(a), the hydrogen can be observed interacting with the nearest, and next-nearest, carbon atoms. However, since the wall of the nanotube curves away from the hydrogen molecule [Fig. 5(b)], the hydrogen is seen to interact with only the nearest carbon atoms. As with graphene, the electron-density change for H_2 at the stable binding separation for site D on the (10, 0) nanotube [Fig. 5(b)] is of the order of 10^{-4} $e/\text{Å}^3$. The weaker interaction between H_2 and the carbon nanotubes can also be observed as, for the same range in electron-density change, the electronic structure of the nanotube is less perturbed compared with the electron structure of graphene when H_2 is at the minimum binding energy at site D [Fig. 5(a)]. Sites A1 and A2 differ negligibly in binding energy for both nanotubes, relative to the spread in adsorption energies. This implies that the length of the nanotubes is adequate to avoid the effects of terminating hydrogen atoms on the molecular hydrogen-nanotube interactions. Therefore, although the simulated nanotubes, used in this study, are unphysically

TABLE III. Separations and binding energies of molecular hydrogen inside the (10, 0) and (9, 0) SWNTs. The separation distances are measured from the nanotube wall to the center of mass of the hydrogen.

	(10, 0)				(9, 0)			
	LDA functional		GGA functional		LDA functional		GGA functional	
Adsorption site	Sep (Å)	E_{bind} (meV)	Sep (Å)	E_{bind} (meV)	Sep (Å)	E_{bind} (meV)	Sep (Å)	E_{bind} (meV)
A1	3.0	143.15	3.9	52.13	3.2	186.57	3.5	47.63
A2	3.0	142.93	3.9	52.07	3.2	186.37	3.5	47.41
B	2.9	149.87	3.6	50.08	3.1	190.74	3.5	49.69
C	2.9	150.57	3.6	50.24	3.1	190.65	3.5	49.85
D	2.8	157.17	3.7	50.47	3.0	193.17	3.5	49.94
E	2.8	152.41	3.6	50.79	2.9	186.25	3.5	52.84
F	2.8	153.95	3.6	50.69	2.9	188.41	3.5	52.10
G	2.8	156.29	3.6	50.61	2.9	191.88	3.5	50.96

short compared with real nanotubes, they are long enough to accurately reproduce adsorption characteristics to the ability of the DFT functionals used.

A summary plot of the binding energies for all adsorption sites, carbon nanostructures, and for both DFT functionals utilized (Fig. 6) shows that hydrogen adsorption is most stable, and therefore preferable, on graphene at all adsorption sites. The results of Fig. 6 show the general trend that H_2 oriented parallel to the graphitic surfaces is more stable than H_2 oriented perpendicular to the surfaces for all nanostructures. This trend is observed for both DFT functionals employed. The curvature inherent in nanotubes decreases the binding strength due to a decrease in interaction between the hydrogen and the carbon nanostructures, but overall the binding energies only range over 40 meV for the LDA functional and 4 meV for the GGA functional.

Figure 7 shows the potential energy for hydrogen oriented parallel to the (10, 0) nanotube wall (site E), both inside and outside the nanotube. Binding energies rise quickly as the hydrogen nears the nanotube wall due to the rapid increase in the energy of the filled antibonding state between hydrogen and nanotube as discussed before. At 51 meV, the stable binding energy of internally positioned hydrogen is larger than that of externally positioned hydrogen. This is evident in the deeper energy well inside the nanotube (right-hand side of Fig. 7). A distinctive double minimum is seen mirrored across the nanotube axis indicating that H_2 placed at site E achieves a global minimum within the nanotube radius.

Interaction energies for internally adsorbed hydrogen are summarized in Table III. All binding energies are larger for the internal hydrogen bonding compared with the binding energies of hydrogen physisorbed to graphene or outside the nanotubes. The increased binding strength is due to an increase in the amount of interaction between the hydrogen and the nanotube. As observed earlier, externally placed hydrogen interacts significantly with only the nearest carbon atoms on the nanotube wall and with next-nearest neighbors on the graphene sheet. This is due to the increasing distance between carbon and hydrogen atoms. As the nanotube surface curves away from the hydrogen, the carbon-hydrogen distance is increased, thus decreasing the interaction. Conversely, for internally placed hydrogen, the nanotube curves toward the hydrogen, keeping the carbon-hydrogen distances relatively consistent. Changes in the electron density show the hydrogen molecule interacting with a greater number of carbon atoms in both the (10, 0) [Fig. 8(a)] and the (9, 0) [Fig. 8(b)] nanotubes.

The binding energies for the (9, 0) nanotube, calculated using the LDA functional, are stronger than those for the (10, 0) by an average of 40 meV. As the radius of the nanotubes decreases, the curvature of nanotubes increases as the reciprocal of the radius. Although the change in curvature between the two nanotubes studied is small, the cross-sectional area decreases as the square of the radius such that the area decreases faster than the curvature. Therefore, the electronic density inside the nanotube is increased by a greater proportion than when the radius is decreased. Since the hydrogen molecule's electronic structure remains unchanged relative to the nanotube, it interacts with more electrons as the nanotube wall contracts around it. This is observed in the more perturbed state of the (9, 0) nanotube's electron density in Fig. 8(b).

For the LDA calculations, the trend that parallel configurations of the hydrogen molecule are more stable than perpendicular configurations is continued for both the (10, 0) and (9, 0) nanotubes. On average, the binding energies of the parallel configurations are 8 and 1 meV more stable for the (10, 0) and (9, 0) nanotubes, respectively. This indicates a significant reduction in the spread of binding energies compared with the differences in externally positioned hydrogen. Since both hydrogen atoms are in close proximity to more carbon atoms inside the nanotube than outside, the effect of

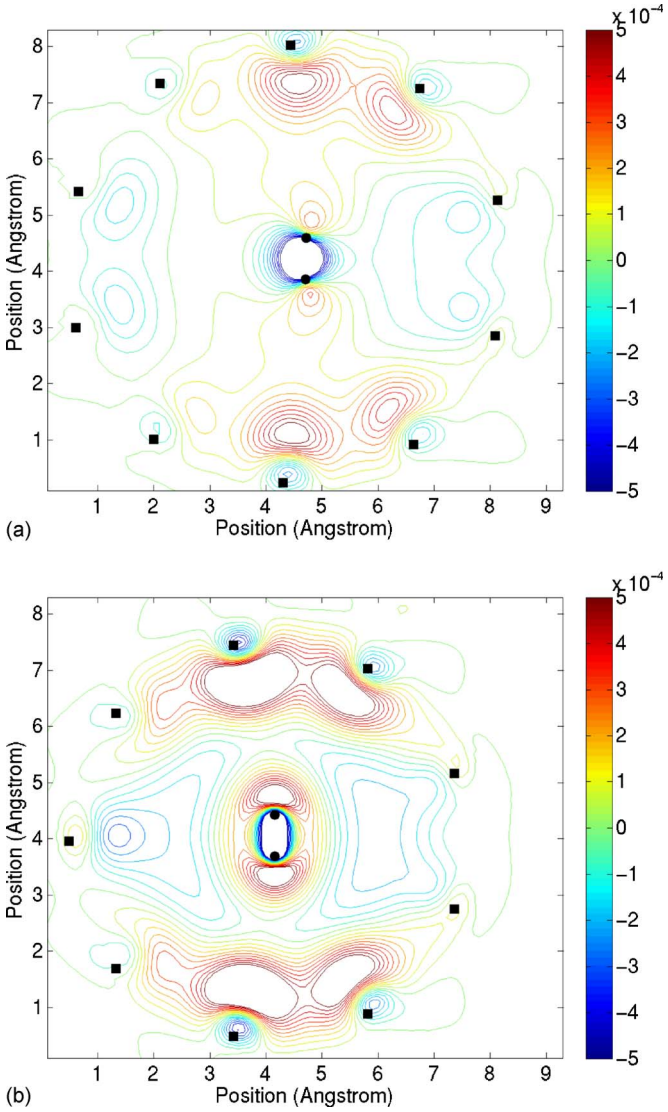

FIG. 8. (Color online) Contour map of the change in electron density for a hydrogen molecule placed inside (a) the (10, 0) and (b) the (9, 0) nanotube. The hydrogen is positioned 3.5 Å away from the nanotube wall (right-hand side of the contour plots) parallel to the surface and the nanotube equator (adsorption site D). Hydrogen atoms are labeled by black circles, while C–C bonds are labeled by black squares that correspond to the nanotube wall. The view is looking down the nanotube axis with the nanotube center line to the left of the map. Scale bar is in units of $e/Å^3$.

the change in orientation of the hydrogen molecule is negated by the increased interaction between the H_2 and the nanotube. The difference in average binding energies between parallel and perpendicular hydrogen, placed external to the nanotubes, varies insignificantly between the (10, 0) and (9, 0) nanotubes. By contrast, the average binding energies for internally placed hydrogen differ by 7 meV between nanotubes, further evidence that as the nanotube radius decreases the increased interaction surpasses the effect of the change in H_2 orientation. Stable binding sites are found at separations less than the nanotube's radius from the nanotube wall, for both nanotubes studied. The GGA functional does not show stable binding at separations less than the radius of the (9, 0) nanotube. All the binding-energy minima for the (9, 0) nanotube are found to lie on the tube axis: the position of balanced repulsion forces from both sides of the nanotube as opposed to a balance between attractive and repulsive forces. Stable binding is found for the (10, 0) nanotube on all sites except for the hydrogen molecule approaching the wall above a carbon atom (sites A1 and A2).

As the vdW corrected, binding-energy, values for H_2 on graphene occur between the LDA and GGA results presented earlier, a general rule can be applied to hydrogen physisorption on the internal surfaces of nanotubes with varying radii. If both LDA and GGA calculations show stability at the tube axis, then hydrogen will only bind at the axis of a nanotube. Hydrogen will bind with hydrogen-nanotube wall separations less than the nanotube's radius if both LDA and GGA calculations show stability within the nanotube radius. The hydrogen molecule may bind within the nanotube's radius when the LDA functional shows stability and the GGA does not.

The results of the DFT calculations presented here show that hydrogen molecules placed inside carbon nanotubes exhibit the strongest physisorption compared with the results for externally placed hydrogen and graphene. This is due to an increased interaction between the hydrogen and the carbon atoms in the nanotube wall. The size of the nanotube, and therefore the curvature, significantly affects the binding strengths in contrast with externally placed hydrogen. If H_2 can bind within the nanotube radius, then the trend of parallel configurations being more stable than perpendicular configurations still applies. However, the internal hydrogen binding energies, although the strongest found here, are still small compared to covalent bonds. Therefore, it is unlikely that hydrogen molecules will bind to the nanotube walls at practical temperatures.

IV. CONCLUSIONS

In conclusion, molecular hydrogen can bind to carbon nanostructures, such as graphene and carbon nanotubes, with weak binding energies. Small changes in the electron density of the carbon-hydrogen systems reflect the weak binding. Hydrogen is weakly bound by physisorption to the surface of a graphene layer. The binding energies for hydrogen adsorbed onto graphene are larger than for hydrogen adsorbed externally onto the (10, 0) and (9, 0) nanotubes. There is no discernible difference between the external binding energies of the nanotubes. This implies that the metallic or semiconducting nature of nanotubes has little effect on hydrogen binding for this size. However, the curvature difference between the (10, 0) and (9, 0) nanotubes has a significant effect on the internally bound hydrogen. Hydrogen placed inside the nanotube has a larger binding energy than both graphene and externally bound hydrogen, by a factor of approximately 2. The curvature of the nanotubes has not affected the binding energies of externally adsorbed hydrogen; however, the binding energies of internally adsorbed hydrogen are affected by curvature. Hydrogen oriented parallel to the surface of the carbon structures is generally found to be more stable than hydrogen oriented normal to the carbon surfaces, due to the ellipsoidal nature of the hydrogen electronic structure. The weak binding energies show that hydrogen adsorption and delivery are energetically viable compared with chemisorption. Operating temperatures of such a system will need to be low as the potential-energy barriers will be easily overcome by thermal agitation at room temperatures.

ACKNOWLEDGMENTS

The authors acknowledge funding from the Engineering and Physical Sciences Research Council, UK.

*Electronic address: d.henwood@surrey.ac.uk

†Electronic address: david.carey@surrey.ac.uk

[1] M. S. Dresselhaus, *Basic Research Needs for the Hydrogen Economy*, 2nd ed. (Office of Basic Energy Sciences, U.S. Department of Energy, Washington, DC, 2004).

[2] International Energy Agency, *Hydrogen & Fuel Cells* (Organisation for Economic Co-operation and Development, Paris, 2005), p. 75.

[3] G. Guella, C. Zanchetta, B. Patton, and A. Miotello, J. Phys. Chem. B **110**, 17024 (2006).

[4] B. Bogdanović and G. Sandrock, MRS Bull. **27**, 712 (2002).

[5] Y. Kojima, Y. Kawai, and Haga, J. Alloys Compd. **424**, 294 (2006).

[6] R. A. Varin, T. Czujko, C. Chiu, and Z. Wronski, J. Alloys Compd. **424**, 356 (2006).

[7] S. K. Bhatia and A. L. Myers, Langmuir **22**, 1688 (2006).

[8] A. C. Dillon, K. M. Jones, T. A. Bekkedahl, C. H. Klang, D. S. Bethune, and M. J. Heben, Nature (London) **386**, 377 (1997).

[9] S. Hynek, W. Fuller, and J. Bentley, Int. J. Hydrogen Energy **22**, 601 (1997).

[10] Y. Ye, C. C. Ahn, C. Witham, B. Fultz, J. Liu, A. G. Rinzler, D. Colbert, K. A. Smith, and R. E. Smalley, Appl. Phys. Lett. **74**, 2307 (1999).

[11] C. Liu, Y. Y. Fan, M. Liu, H. T. Cong, H. M. Cheng, and M. S. Dresselhaus, Science **286**, 1127 (1999).

[12] J. S. Arellano, L. M. Molina, A. Rubio, M. J. Lopez, and J. A.

Alonso, J. Chem. Phys. **117**, 2281 (2002).
[13] Y. Okamoto and Y. Miyamato, J. Phys. Chem. B **105**, 3470 (2001).
[14] J. S. Arellano, L. M. Molina, A. Rubio, and J. A. Alonso, J. Chem. Phys. **112**, 8114 (2000).
[15] M. K. Kostov, H. Cheng, A. C. Cooper, and G. P. Pez, Phys. Rev. Lett. **89**, 146105 (2002).
[16] H. Cheng, G. P. Pez, and A. C. Cooper, J. Am. Chem. Soc. **123**, 5845 (2001).
[17] S. S. Han and H. M. Lee, Carbon **42**, 2169 (2004).
[18] X. Xu, Q. S. Zhang, R. P. Muller, and W. A. Goddard, J. Chem. Phys. **122**, 014105 (2005).
[19] P. Giannozzi, R. Car, and G. Scoles, J. Chem. Phys. **118**, 1003 (2003).
[20] P. Lazic, Ž. Crljen, R. Brako, and B. Gumhalter, Phys. Rev. B **72**, 245407 (2005).
[21] A. W. C. van den Berg, S. T. Bromley, J. C. Wojdel, and J. C. Jansen, Phys. Rev. B **72**, 155428 (2005).
[22] M. Khantha, N. A. Cordero, L. M. Molina, J. A. Alonso, and L. A. Girifalco, Phys. Rev. B **70**, 125422 (2004).
[23] A. J. Du and S. C. Smith, Nanotechnology **16**, 2118 (2005).
[24] S. Rigamonti and C. R. Proetto, Phys. Rev. B **73**, 235319 (2006).
[25] Dmol^3 is a registered software product of Accelrys Software Inc.
[26] S. J. Vosko, L. Wilk, and M. Nusair, Can. J. Phys. **58**, 1200 (1980).
[27] J. P. Perdew and Y. Wang, Phys. Rev. B **45**, 13244 (1992).
[28] J. P. Perdew, K. Burke, and M. Ernzerhof, Phys. Rev. Lett. **77**, 3865 (1996).
[29] G. W. C. Kaye, *Tables of Physical and Chemical Constants*, 16th ed. (Longman, Harlow, 1995), p. 273.
[30] A. R. Ubbelohde, *Graphite and its Crystal Compounds* (Clarendon, Oxford, 1960), p. 5.
[31] H. O. Pierson, *Handbook of Carbon, Graphite, Diamond, and Fullerenes: Properties, Processing and Applications* (Noyes, Park Ridge, NJ, 1993), p. 45.
[32] D. Henwood and J. D. Carey (unpublished).